IEEE Access
Multidisciplinary | Rapid Review | Open Access Journal

Received February 5, 2021, accepted February 21, 2021, date of publication February 26, 2021, date of current version March 18, 2021.

Digital Object Identifier 10.1109/ACCESS.2021.3062375

Path Planning and Obstacle Avoiding of the USV Based on Improved ACO-APF Hybrid Algorithm With Adaptive Early-Warning

YANLI CHEN[1], GUIQIANG BAI[1], YIN ZHAN[1], XINYU HU[1], AND JUN LIU[2,3], (Student Member, IEEE)

[1]Key Laboratory of CNC Equipment Reliability, Ministry of Education, School of Mechanical and Aerospace Engineering, Jilin University, Changchun 130022, China
[2]School of Computer Science and Technology, Jilin University, Changchun 130022, China
[3]School of Electronics and Information Engineering, Beihang University, Beijing 100191, China

Corresponding authors: Guiqiang Bai (baigq19@jlu.edu.cn) and Yin Zhan (1064280920@qq.com)

This work was supported in part by the Jilin Province Key Science and Technology Research and Development Project under Grant 20180201040GX, in part by the Aeronautical Science Foundation of China under Grant 2019ZA0R4001, in part by the National Natural Science Foundation of China under Grant 51505174, in part by the Scientific and Technological Development Program of Jilin Province of China under Grant 20170101206JC, in part by the Foundation of Education Bureau of Jilin Province under Grant JJKH20170789KJ, in part by the Doctoral Program of Higher Education of China under Grant 20130061120038, and in part by the National Key Research and Development Program of China under Grant 2017YFC0602002.

ABSTRACT Path planning is important to the efficiency and navigation safety of USV autonomous operation offshore. To improve path planning, this study proposes the improved ant colony optimization-artificial potential field (ACO-APF) algorithm, which is based on a grid map for both local and global path planning of USVs in dynamic environments. The improved ant colony optimization (ACO) mechanism is utilized to search for a globally optimal path from the starting point to the endpoint for a USV in a grid environment, and the improved artificial potential field (APF) algorithm is subsequently employed to avoid unknown obstacles during USV navigation. The primary contributions of this article are as follows: (1) this article proposes a new heuristic function, pheromone update rule, and dynamic pheromone volatilization factor to improve convergence and mitigate finding local optima with the traditional ant colony algorithm; (2) we propose an equipotential line outer tangent circle and redefine potential functions to eliminate goals unreachable by nearby obstacles (GNRONs) and local minimum problems, respectively; (3) to adapt the USV to a complex environment, this article proposes a dynamic early-warning step-size adjustment strategy in which the moving distance and safe obstacle avoidance range in each step are adjusted based on the complexity of the surrounding environment; (4) the improved ant colony optimization algorithm and artificial potential field algorithm are effectively combined to form the algorithm proposed in this article, which is verified as an effective solution for USV local and global path planning using a series of simulations. Finally, in contrast to most papers, we successfully perform field experiments to verify the feasibility and effectiveness of the proposed algorithm.

INDEX TERMS Unmanned surface vehicles (USVs), path planning, improved ant colony optimization-artificial potential filed (ACO-APF) algorithm, unknown obstacle avoidance, field experiment.

I. INTRODUCTION

Interest in the path-planning and collision-avoidance problems of unmanned ground vehicles (UGVs), unmanned surface vehicles (USVs), and unmanned aerial vehicles (UAVs) has grown over the past decade [1], [2]. USVs can be defined as unmanned vehicles that can navigate on water with automatic algorithms or remote control measures. With the development of artificial intelligence and sensor technology, USVs applications have become increasingly diverse and now include scientific research, oceanographic surveys, marine salvage, military use, and military use [3]–[6]. These tasks are related to target recognition, path planning, control technology, positioning and navigation technology, communication

The associate editor coordinating the review of this manuscript and approving it for publication was Yongqiang Cheng.

technology [7]. The limited energy capacity of USVs and the complex surface environments they face with regard to navigation paths and arrival times make path planning and obstacle avoidance critical to USVs, which requires a certain level of intelligence in USVs [8].

Path planning aims to calculate the shortest collision-free path from the start to the endpoint by avoiding static and dynamic obstacles under the constraints of safety, energy consumption, and/or time. Path planning is typically divided into global and local path planning based on what type of environmental information is known [9]. A known environment indicates that all information about obstacles and targets is known prior to launching a USV, and the vehicle plans its path navigation based on this prior knowledge, which primarily includes the visual graph method, cell decomposition, the A* algorithm, and the grid method [10]–[13]. Conversely, in unknown environments, vehicles know nothing or only some information about their environment prior to launch, and local path planning is primarily performed by artificial potential field methods, genetic algorithms and simulated annealing [14]–[16]. However, in the path planning of USVs, all these algorithms have strengths and weaknesses. For example, the A* algorithm is easy to use but not suitable for dynamic path planning [17]; the grid algorithm is easy to understand but strongly affected by the environment and inflexible [18]; and the genetic algorithm cannot solve multiple obstacles [12]. In recent years, path planning techniques based on simultaneous localization and mapping (SLAM) have gradually become market-based [19]–[21]. The construction of the SLAM technology environment map relies on precise localization, which in turn depends on the accurate environment map [20]. Due to the influence of ocean background light and suspended turbidity particles, SLAM technology has a short detection distance and poor real-time performance. SLAM technology thus remains a long way from being applied in practical application of ocean path planning [23], [24]. In a marine environment, particularly on the surface, where unmanned vessels operate, GPS has the advantage of high positioning accuracy, and RTK can achieve a positioning accuracy of a few centimeters. GPS is less affected by the marine environment and can thus determine the absolute position of the USV. Because the USV working environment is known, the absolute position of obstacles can be shown on a map. Therefore, a USV can determine its absolute position on the map at all times via GPS, in which the sample frequency is typically 2∼5 Hz, which is faster than SLAM; thus, GPS is used in this study.

Relative to autonomous underwater vehicles (AUVs), USVs can easily take advantage of existing navigation charts. However, due to the limitations of sensors and communication conditions, USVs cannot rely solely on existing charts to fully access global information when faced with complex marine environments and navigation conditions, which leads to their inability to perform safe path planning; thus, the validity and reliability of path planning is a great challenge. Therefore, a realistic scheme for USV path planning is to use local sensor information to plan a path based on global path planning [25]. In recent years, many researchers have presented several comprehensive planning methods with complementary advantages based on the features of global and local path planning, and several important results have been achieved. Sgorbissa and Zaccaria [26] proposed a hybrid path-planning approach that integrates prior knowledge with local sensor information to achieve specific goals. When a USV is running in a partially unknown environment, the algorithm can ensure that the robot will not fall into a deadlock; however, the system relies heavily on local awareness and navigation strategies. Lazarowska [27] proposed the discrete artificial potential field (DAPF) algorithm so that a USV can effectively avoid static and dynamic obstacles during path planning. Thus, Montiel *et al.* [28] constructed an APF algorithm unified with the bacterial evolutionary algorithm, which improves the planning flexibility and has a good verification effect compared to the traditional potential field method. Zhao [29] proposed a path-planning algorithm that combines cooptimization of the multiobjective Cauchy mutation cat swarm optimization (MOCMCSO) and artificial potential field (APF) to quickly search globally and describe optimal path planning while modifying APF parameters to adapt to different environments and dynamic obstacles. Shuang *et al.* [30] combined the pheromone updating rules of the ACO algorithm with the searching mechanism of the particle swarm algorithm to achieve a balance between exploration and development and improve search efficiency. Tsou [31] used the ACO algorithm, automatic identification system information, and obstacle avoidance rules for USV dynamic path planning. This algorithm uses local static obstacles and a dynamic programming model to equilibrate the preponderance of global and local path planning. Zhang and Chen [32] combined the ACO algorithm and artificial potential field method to construct local-inspired pheromones based on the value and direction of the potential field force that ants were subjected to in the environment. Additionally, Zhao and Yi [33] introduced the influence coefficient of potential field force-inspired information to improve the quality of the solution. However, the convergence speed of this algorithm is affected by the fact that the constructed local pheromones have no internal relationship with the global pheromones, and the smoothness is poor. Tsou noted that if the ACO algorithm can increase the convergence speed with large maps, large-scale obstacle path-planning problems could be solved more accurately [31]. Therefore, many researchers have proposed an improved ant colony algorithm [17], [34]–[36] to improve the convergence speed and the ability to search for an optimal path. For example, Che and Han *et al.* APF is relatively simple mathematically, easy to understand, and highly efficiency, and can play a critical role in USV dynamic obstacle avoidance [18]. Although APF is insufficient in the case of multiple obstacles and complex movements, this theory can still be improved and applied to practical problems [14]. To the best of our knowledge, collision-free large-scale outdoor sea trials about

USV path planning have not been reported in the literature to date.

II. PROBLEM STATEMENT

Motivated by the facts and challenges stated above, we propose an improved ACO-APF hybrid algorithm that can describe the shortest time path planning for USVs in an unknown environment without collisions. On the path-planning level, a USV is considered a point-mass system, and the dynamic model of the USV is a single integrator. This article primarily provides the following three contributions:

a) To use USV global path planning, an improved ACO algorithm is proposed to improve the heuristic function, pheromone updating mode, and pheromone volatile factor of the traditional algorithm to improve the efficiency and quality of path searching and convergence.

b) We propose the improved APF algorithm. First, we reconstruct the repulsion potential field function to solve the GNRON problem. Second, we propose the "equipotential line tangent circle escape" method to solve the local minimum and dynamic obstacle problems successfully. Due to the complexity of the environment, this article proposes a dynamic step size adjustment strategy to allow the USV to adapt to a complex environment.

c) To describe USV autonomous path planning based on the USV's maneuvering capability and the radar sensitive range, a dynamic early-warning mechanism is designed, a reasonable path planning step size is chosen in terms of the density of obstacles, and the dynamic search path is smoothed. The organic integration of global path planning and local dynamic obstacle avoidance is also achieved.

This article is organized as follows. In Section II, the environment and USV model as well as the basic formulae of the traditional ACO algorithm and APF method are introduced. The primary research contents and results are provided in Section III. In Section IV, the proposed algorithms are simulated to verify their effectiveness and feasibility. Experiments are performed on a real USV platform in Section V. Finally, conclusions are drawn in Section VI.

III. ENVIRONMENTAL MODEL AND BASIC ALGORITHM

A. ENVIRONMENTAL MODELING

In this article, we assume that a USV is working and moving in a general two-dimensional [Please note that the font changes here. Please consider using a consistent font type and size throughout the manuscript.](2-D) plane workspace. In terms of path planning, a grid diagram is frequently used to build a static environment [37]. Grids are numbered from top to bottom, left to right, where starting and target points are the top left corner S point and the bottom right corner G point. The black grid represents obstacles, such as islands, rocks, floatage, and ships; and counts obstacles that are one grid away as too close for the safety. The white space represents the navigable area, and each grid length is set as a unit of distance. Considering the USV's size, speed, and

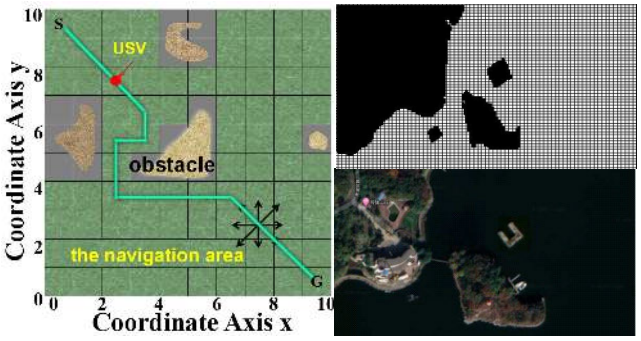

FIGURE 1. Environmental model (a) Grid diagram (b) The experimental area grid.

maneuverability, the grid scale is shown in Equation 1:

$$L_g = \varsigma L_{USV} + \bar{V}_{USV} \cdot t_g \tag{1}$$

where L_{USV} is the characteristic length of USVs, $\bar{V}$ is the average speed of the USV, t_g is the sailing time of the USV in one grid, and ζ is the coefficient of the Fujii obstacle avoidance model [38]. The grid coding method of the raster graph is the coordinate, and the encoding and coordinates (x, y) in the graph correspond as shown in equation 2.

$$\begin{cases} x = \mathrm{mod}(c, n) - 0.5 \\ if\ x = -0.5, x = 19.5 \\ y = n + 0.5 - ceil(c/n) \end{cases} \tag{2}$$

where c and n are the coded value of the grid and the number of grids in each row, respectively, and *ceil* is the rounding operation.

The USV is viewed as a mass point that can move in eight directions from its current position to eight adjacent grids, as shown in Figure 1(a). Figure 1(b) shows a binary raster diagram of the experimental water area developed by the grid method. The raster diagram cannot show the outline of obstacles in detail but reduces the difficulty of dynamic path planning. Before beginning navigation, the chart modeled by the raster method is input into the USV controller, after which global path planning is performed. The USV uses GPS to obtain its position information during navigation..

B. THE USV MODEL

Different from UGVs and UAVs, USVs have low mobility and require a large safety obstacle avoidance distance. The altitude of a USV will fluctuate due to wave action; however, this motion is negligible compared to the USV's in-plane motion and can thus be ignored. We thus only consider motion in a two-dimensional plane. For USV navigation, inner and outer ring structures can be used to describe the navigation of USVs if the path is only related to the USV's position [39], [40]. In this configuration, the outer ring is used to drive the USV toward the desired position, while the inner ring can be used to control the attitude. This article primarily provides the location information required for the outer ring control of the USV. At the path-planning level, the USV can

be considered to be a point. The detailed relationship model between USVs and obstacles is shown in Section III.

C. TRADITIONAL ANT COLONY AND APF ALGORITHM

1) TRADITIONAL ANT COLONY ALGORITHM

The principle of the ACO algorithm is to treat each USV as an ant. In the basic ACO algorithm, the feasibility of ant k from the current grid i to the next j at the moment t is given in Equation (3):

$$p_{ij}^{k}(t)=\begin{cases}\tau_{ij}^{\alpha}(t)\eta_{ij}^{\beta}(t)/\left(\sum\limits_{s\in allowed_k}\tau_{is}^{\alpha}(t)\eta_{is}^{\beta}(t)\right) & j\in allowed_k\\ 0 & \text{others}\end{cases} \tag{3}$$

where $allowed_k$ indicates the free grid that the ant can choose next, $\tau_{ij}(t)$ indicates the pheromone content between the grid i and j at t-moment, α is the pheromone heuristic factor, and β is the expected heuristic factor, and $\eta_{ij}(t)$ is the expected heuristic function from the grid i to j at t-moment, which can be expressed as follows.

$$\eta_{ij}(t)=1/\|p_i-p_j\| \tag{4}$$

where $\|\bullet\|$ is the Euler distance of grids i and j, and p_i and p_j are mean the coordinates of the grid.

While searching for an optimal path, ants leave new pheromones along each path they take, which changes with the passage of time and the number of ants. The rules that govern these changes are shown in Equations (5):

$$\begin{cases}\tau_{ij}(t+1)=(1-\rho)\tau_{ij}(t)+\Delta\tau_{ij}(t)\\ \Delta\tau_{ij}(t)=\sum\limits_{k=1}^{m}\Delta\tau_{ij}^{k}(t)\end{cases} \tag{5}$$

where ρ represents the pheromone volatilization factor, whose value range is (0,1), and $(1-\rho)$ indicates the pheromone residual factor, and $\Delta\tau_{ij}^{k}(t)$ is the pheromone increment left by the kth ant at time t between grids i and j after this search, and equals 0 initially.

2) TRADITIONAL APF ALGORITHM

The APF algorithm is an abstract description of both target and obstacle points in the water. The algorithm constructs gravitational and repulsive potential field functions to represent the impact of obstacles and targets in circumstances of USV. The potential field of any point in the environment is the superposition of the gravitational and repulsive potential fields. The force acting on this point is the vector sum of the negative gradients of the gravitational and repulsive potential fields. The USV plans a noncollision path and moves to the target point by searching for the direction in which the potential field function decreases. The attractive potential field functions U_{att} and repulsion potential field functions U_{rep} are defined as follows.

$$\begin{cases}U_{att}(q)=0.5k_{att}\left\|q-q_g\right\|^2\\ U_{rep}(q)=0.5k_{rep}(1/\left\|q-q_o\right\|-1/d_0)^2\end{cases} \tag{6}$$

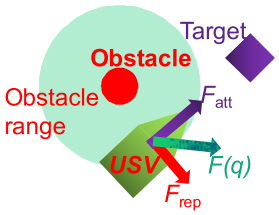

FIGURE 2. The resultant force F(q) schematic diagram.

where k_{att} and k_{rep} are the gain coefficients of the attractive and repulsion field functions, respectively; q is the coordinate of the USV; q_g is the target coordinate; and d_0 is the influence range of the obstacles.

The resultant potential field function $U(q)$ is defined as the sum of the gravitational and the repulsion potential field functions, and the resultant force $F(q)$ to USV is defined as follows. The resultant force $F(q)$ schematic diagram is shown in Figure 2.

$$\begin{aligned}F(q)&=F_{att}(q)+F_{rep}(q)=-\nabla U_{rep}(q)-\nabla U_{att}(q)\\&=-\nabla U(q)\end{aligned} \tag{7}$$

where $F_{att}(q)$ and $F_{rep}(q)$ are the attractive and repulsion forces, respectively.

Based on these description of the traditional ACO algorithm and APF algorithm, the traditional ACO algorithm converges more slowly and tends to become stuck at local optima, which may make the target unreachable. Therefore, this article combines two algorithms to perform USV path planning while focusing on these problems.

IV. ALGORITHM ANALYSIS AND MAIN RESULTS

A. IMPROVED ACO ALGORITHM

1) IMPROVING OF THE HEURISTIC FUNCTION

In the traditional ACO algorithm, the heuristic function only consider the current node i and the next node j, and does not take a full account to the initial point S and the target point G, which may cause the algorithm to deadlock when selecting the next node, resulting in the algorithm stagnation. The heuristic function is improved as in Equation (8) :

$$\eta_{ij}(t)=d_{Sj}/\left(d_{ij}+d_{jG}\right) \tag{8}$$

where d_{Sj} represents the distance between the initial point S and the next node j, and d_{jG} is the distance between the node j and the target point G.

Based on Equation (8), the farther from the point S and the closer to the point G, the larger the d_{Sj} value and the smaller the d_{jG} value will be, resulting in a greater probability that node j will be selected. The improved heuristic function moves the ant away from the initial point and closes to the target when selecting the next node to prevent the algorithm from getting stuck in a deadlock.

2) IMPROVED PHEROMONE UPDATE RULES

In the initial phase of searching, the conventional ACO algorithm will search for certain suboptimal paths. If the

pheromones of these paths are updated every time, it will mislead subsequent ants and slow down the convergence of the optimal path or even lead to nonconvergence..

After these improvements, the pheromone update rule becomes "reduce the pheromone content along the poor path in the later phase of the algorithm exploration so that the ants do not choose this path", which increases the convergence speed of the algorithm. The pheromone update rule changed to Equation (9):

$$\Delta\tau_{ij}^{k}(t) = \begin{cases} Q/L_k & N_c < A \\ Q/\left(L_{mid} - L_k\right) & N_c \geq A \end{cases} \tag{9}$$

where Q represents the pheromone concentration; L_k signifies the total length of the path traversed by the kth ant after completing the cycle; L_{mid} is the average of the total search path length of all ants after one iteration; N_c is the number of iterations; and A is a constant related to the number of iterations.

3) IMPROVING THE PHEROMONE VOLATILIZATION FACTOR

In the ACO algorithm, the pheromone volatilization factor is an important parameter. If it is too large, the residual pheromones on the path will volatilize too quickly and thus cannot embody the positive feedback of the ACO algorithm and hinders convergence. Conversely, pheromones will be kept on the path for a long time, resulting in the algorithm finding a local optima. Therefore, this article proposes the dynamic pheromone volatilization factor. In the initial phase of the algorithm, a large pheromone volatilization factor is used to advance the search scope of ants to improve the search efficiency. In the later stage, a small pheromone volatilization factor is used to accelerate the convergence rate of the algorithm. The pheromone volatile factor decreases with increasing iterations and is updated based on Equation (10):

$$\rho = \rho_{\max} - N\left(\rho_{\max} - \rho_{\min}\right)/N_{\max} \tag{10}$$

where $\rho_{\max}$ and $\rho_{\min}$ respectively indicate the max and min values of pheromone volatilization factors, respectively; and N and $N_{\max}$ respectively indicate the current and maximum number of iterations, respectively.

Based on these three measures, the disadvantages of the traditional ACO algorithm are effectively solved, and the search efficiency and success rate are improved.

B. IMPROVED APF METHOD

1) DYNAMIC EARLY-WARNING OBSTACLE AVOIDANCE MODEL

During USV navigation, uncharted obstacles, such as floatage and ships, may be encountered and will affect navigation safety. Therefore, local path planning must be performed. Local path planning based on sensor information can be performed in real time and is highly practicable. After a sensor detects an uncharted obstacle, the relative position of the obstacle related to the USV is added to the global map for obstacle avoidance. The relative position relationship

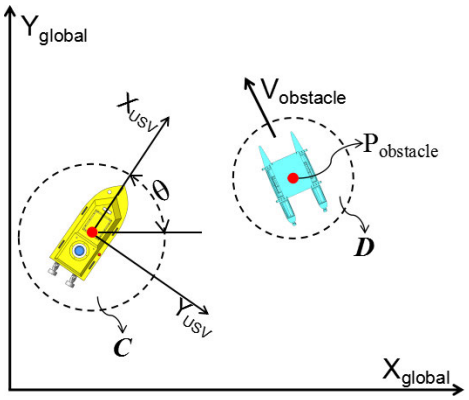

FIGURE 3. The location with the USV and obstacles.

between the obstacle and the global coordinate system is shown below:

$$P_{obstacle} = \begin{bmatrix} X_{obstacle} \\ Y_{obstacle} \end{bmatrix} = \begin{bmatrix} X_{USV} \\ Y_{USV} \end{bmatrix} + \begin{bmatrix} \cos\theta & -\sin\theta \\ \sin\theta & \cos\theta \end{bmatrix} \times \begin{bmatrix} P_{x-obstacle} \\ P_{y-obstacle} \end{bmatrix} \tag{11}$$

where $P_{obstacle}$ and P_{UsV} are the positions of obstacles and USVs in the global coordinate system, respectively. θ is the heading Angle of the USV; and $P_{y\text{-}obstacle}$ and $P_{x\text{-}obstacle}$ are the positions of the obstacle in USV coordinates. In the selection of the USV obstacle avoidance range, emphasis should be placed on factors that include inertia and waves. We define the USV's obstacle avoidance area and obstacle influence range as C and D respectively, where C is a circle with the center of mass of the USV as the center of the circle, S is its the radius, and D is a circle with the obstacle as the center and the radius as Q:

$$\begin{cases} S = d - \delta L_{USV}/\mu \\ Q = \xi L_{obstacle} \end{cases} \tag{12}$$

where d is the detection range of the sensor, L_{USV} and $L_{obstacle}$ are respectively the USV and obstacle characteristic length, respectively; δ and ξ are the coefficients related to USV and obstacle velocity respectively with a value range of (1, 3); and μ is a coefficient related to sea conditions that depends on the roll angle and pitch angle fluctuations during the USV navigation with a value range of (0, 1). The relationship between USV and obstacles should follow Equation 13, and the relationship between the USV and the location of obstacles is shown in Figure 3:

$$\|P_{usv} - P_{obstable}\| \geq S + Q \tag{13}$$

During navigation, an inner ring PID controller, as described in [41], [42], is used to control the USV so that it can maintain the desired trajectory while also maintaining a safe distance from obstacles. USVs use different avoidance courses when encountering obstacles in different directions. Additionally, to ensure that the USV is controllable, the maximum USV rotation angle $\alpha_{\max}$ shall meet the following

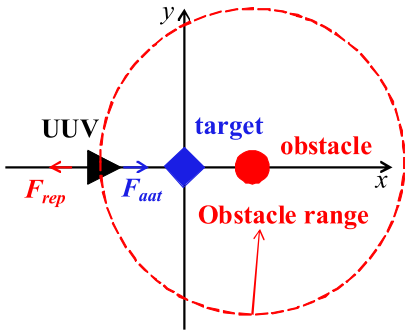

FIGURE 4. GNRON position relation.

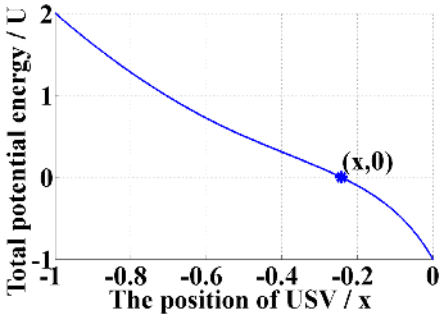

FIGURE 5. The USV Potential energy of traditional APF.

requirements:

$$\alpha_{\max} = \pi/2 - \arccos\left((S+Q)/R_{\min}\right) \tag{14}$$

2) IMPROVING THE POTENTIAL FIELD FUNCTION FOR GNRON

In the traditional algorithm, as a USV approaches the target point, gravity decreases. When the target point is within the coverage of the obstacle, the repulsive force of the obstacle will be greater than the attraction force of the target on the USV, making the USV fail to reach the target. Based on these assumptions, Figure 4 shows that the positions of the USV, target point and obstacle are (x, 0), (0, 0), and (0.5, 0), respectively. The combined potential energy formed by gravitational F_{aat} and repulsive F_{rep} is shown in Figure 5, which shows that the resultant potential energy of the USV at $x = x$ is zero, and the sign of the resultant potential energy only indicates the direction of the resultant potential energy. Therefore, the resultant potential energy of other positions is greater than this point; thus, the USV oscillates at $x = x_0$ and cannot move to the target point.

Because the repulsion force of obstacles near the target point is not zero, the USV will fail to reach the target precisely. To solve the GNRON problem, the function of the repulsion potential field is improved to make the attraction and repulsion forces at the target position zero so that the USV will move to the target position. The improved Equation (15) is as follows:

$$U_{rep}(q) = \begin{cases} \frac{1}{2}k_{rep}(1/\|q-q_o\| - 1/d_0)^2 d^n(q,q_g) \\ \quad \|q-q_o\| < d_0 \text{and} \left\|q-q_g\right\| < \|q-q_o\| \\ 0 \quad \|q-q_o\| > d_0 \end{cases} \tag{15}$$

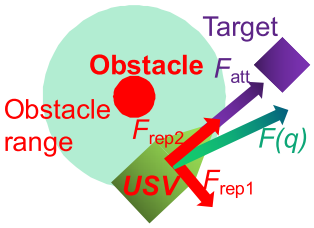

FIGURE 6. The improved force of USV.

TABLE 1. The value of improved repulsion field function.

n	$\vec{F}_{rep1}(q)$	$\vec{F}_{rep2}(q)$	$\vec{F}_{rep}(q)$
0	Same as the traditional algorithm		
(0,1)	0	>0	$\vec{F}_{rep2}(q)$
1	0	$-0.5k_{rep}(1/\|q_o-q\|-1/d_0)$	$\vec{F}_{rep2}(q)$
(1,∞)	0	0	0

The repulsion force generated by the improved function of the repulsion potential field is expressed as Equation (16):

$$\begin{aligned} \vec{F}_{rep}(q) &= -\nabla U_{rep}(q) \\ &= \begin{cases} \vec{F}_{rep1}(q) + \vec{F}_{rep2}(q) \\ \quad \|q-q_o\| < d_0 \text{and} \left\|q-q_g\right\| < \|q-q_o\| \\ 0 \quad \|q-q_o\| > d_0 \end{cases} \end{aligned} \tag{16}$$

where $F_{rep1}(q)$ and $F_{rep2}(q)$ are the forces contained in the improved repulsion potential field function. Equations (17) and (18) will introduce the calculation formula of these two forces:

$$\begin{aligned} \vec{F}_{rep1}(q) = k_{rep}&\left(\frac{1}{\|q_o-q\|} - \frac{1}{d_0}\right)\frac{1}{\|q_o-q\|^2}\left\|q_g-q\right\|^n \\ &\times \frac{\partial\|q_o-q\|}{\partial x} \end{aligned} \tag{17}$$

where $F_{rep1}(q)$ is the component of the repulsion force, whose direction is from the obstacle to the USV, and:

$$\begin{aligned} \vec{F}_{rep2}(q) = -\frac{nk_{rep}}{2}&\left(\frac{1}{\|q_o-q\|} - \frac{1}{d_0}\right)^2\left\|(q_g-q)\right\|^{(n-1)} \\ &\times \frac{\partial\left\|(q_g-q)\right\|}{\partial x} \end{aligned} \tag{18}$$

where $F_{rep2}(q)$ is the second component of the repulsion force, whose direction is that the USV points to the target point, The improved USV is shown in Figure 6, and a comparison of Figures 2 and 6 show that the USV force is significantly improved.

Based on Equations (16) ∼ (18), when the USV approaches the target point, that is, $\lim \left\|q_g - q\right\| \to 0$, the $\vec{F}_{rep}(q)$ value is closely related to n, as shown in the following Table 1.

By analyzing the value of parameter n, it shown that when n is greater than 1, as the USV approaches the target point, both the gravitational and repulsive forces it receives tend toward

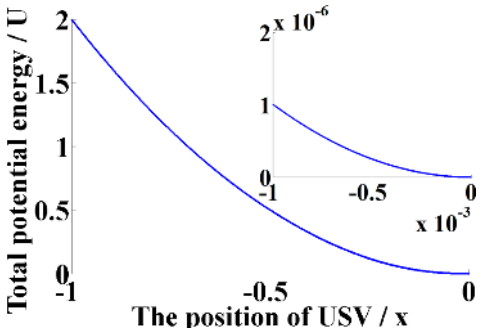

FIGURE 7. The USV Potential energy with the improved APF.

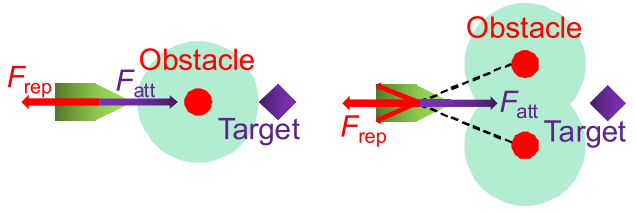

FIGURE 8. Local minimum.

zero, thus solving the problem that the potential energy at the target point is not minimized. The improved potential energy function is used to solve the potential energy received by the USV in Figure 5, and the result is shown in Figure 7, which indicates that the improved function solves the problem of the unapproachable target.

3) THE PROBLEM OF LOCAL MINIMUM

The point at which the USV is subjected to the same gravity and repulsion force and opposite direction in space is the local minimum point, and the resultant force received by the USV at this point is zero, resulting in the USV being unable to reach the target point. There are two types of local minima: a local minimum caused by a single obstacle, as shown in Figure 8.a; and a local minima caused by multiple obstacles, as shown in Figure 8.b. In the first case, mature methods, such as the virtual target point method, could be used. However, the second case is rarely studied; thus, this article analyzes the second case but is equally important.

To solve this problem, we present the "equipotential line tangent circle escape algorithm". If the USV enters the range of influence of an obstacle (i.e., d(q, q0) < d0), then a circle is drawn with the obstacle as the center and the distance from the USV to the obstacle as the radius, with the circle being tangent to the USV. Then, the small arc between the USV's current point position and the tangent point is used as the trajectory of the USV. If the USV is within the range of influence of multiple obstacles, the nearest obstacle to the USV is considered to be the center of the circle, and then the tangent point is determined. Assuming that the slope of the tangent line is k, the equation of the circle and the tangent line in the point-slope form are as follows:

$$y - y_g = k(x - x_g) \tag{19}$$

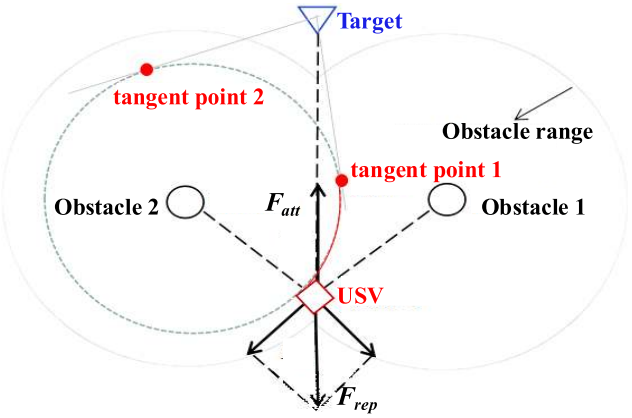

FIGURE 9. Diagram of the proposed algorithm.

$$(x - x_o)^2 + (y - y_o)^2 = r^2 \tag{20}$$

where (x_o, y_o) are the coordinates of the obstacle; (x_g, y_g) are the target coordinates; and r is the distance from the obstacle to the USV.

Based on Equations (19) and (20), the coordinates of the pointcut can be described by follows:

$$\begin{cases} x_c = \left(x_g k^2 + (y_o - y_g)k + x_o\right) \Big/ \left(1 + k^2\right) \\ y_c = \left(y_o k^2 + (x_o - x_g)k + y_g\right) \Big/ \left(1 + k^2\right) \end{cases} \tag{21}$$

The distance from the center of the circle to the tangent line is the radius, and the radius equation can be listed by the formula of the distance from the point to the straight line, as shown in Equation (22):

$$\left(\left| kx_o - y_o + y_g - kx_g \right|\right) \Big/ \left(\sqrt{1 + k^2}\right) = r \tag{22}$$

Equation (22) can be rearranged to obtain Equation (23), as shown at the bottom of the next page.

By substituting Equation (23) into (21), two pointcut coordinates can be obtained, and the pointcut that can form a small arc with the USV's position is selected as the USV's path; thus, pointcut 2 in Figure 7 is the node of the next movement of the USV.

In Figure 9, the resultant force on the USV is zero and encounters a local minima. Using the algorithm in this article, the USV can escape from the local minimum by moving toward tangent point 2 along the red arc in the figure.

After the undiscovered static obstacles in the environment are detected by the USV sensors, the equipotential line outer tangent circle escape method proposed in this article can be used to avoid them. For dynamic obstacles, if the next moving node is the same as the tangent point of the "equipotential line outer tangent circle escape method", the USV will collide with the moving obstacle. Therefore, in the case of dynamic obstacles, the next moving node of the USV is the tangential point that deviates from the movement direction of the obstacle, thus avoiding a collision between the USV and the dynamic obstacles that can be described. Compared to the method reported in [43], the path length planned by the

algorithm in this article is shorter and saves more energy for USVs.

4) STEP SIZE DYNAMIC ADJUSTMENT

Step size is an important parameter of the APF method, and its value is fixed in the proposed method. If the step size is too small, algorithm performance decreases, and the probability of defects in the APF method increases. Conversely, the probability of collision between the USV and obstacle increase. To adapt the USV to a complex environment, this article proposes a dynamic step size adjustment strategy.

After obstacle information is detected by the USV sensor, the USV evaluates the environmental complexity based on the obstacle location information and sets the step size based on the distance between the USV and obstructions. It is assumed that the distance between USV and each obstruction is set $D = \{p1, p2 \ldots, pn\}$; then, the step size is set as follows: (1) if set D is an empty set (i.e., there is no obstacle near the USV), then, the step size value is set to 1; (2) If set D is not an empty set and the minimum value is greater than 1, the step size is set to 1/2 of the minimum value is set D; (3) if set D is not an empty set, and the minimum value is below 1 (i.e., the USV enters the range of influence of obstacles), then the USV avoids obstacles based on the "equal-potential line tangent circle escape algorithm".

C. IMPROVED ACO-APF HYBRID ALGORITHM

Path planning can be split into local and global path planning based on whether environmental information is the acquaintance. There may be an uncharted obstruction in the background, and local path planning is also required when the USV performs global path planning. Therefore, the improved ACO-APF hybrid algorithm is naturally proposed, which is separated into three processes for path planning.

First, global path planning is used to obtain the initial path using the improved ACO algorithm.

Second, the initial path is optimized, as shown in Figure 11 in an example. The initial path planned by the improved ACO algorithm is shown in the red solid line in Figure 8, and the inflection point coordinates from p_1 to p_8 are recorded. The path is then simplified, and the process is as shown below: each inflection point of the path is represented by P_1,P_2,...,P_n, and connects P_1 to P_3. If the line does not pass through the obstacle (i.e., the USV will not collide with the obstacle when moving) then P_1 and P_4 are further connected, and so on, until p_1 and P_m ($m = 3, 4, \ldots$) through the obstacle when connecting, then connect P_1 to P_{m-1}, and the redundant inflection points between P_1 and $P_{m-1}$are removed. These steps are then repeated with the inflection point P_{m-1} as the initial point until there are no redundant inflection points. The simplified path is displayed in the blue dotted line in Figure 10, and the number of simplified inflection points decreases from 8 to 5, which makes the path smoother while reducing the path length.

The third step for local path planning is to use the first inflection point P_4 as an initial point, the second inflection point P_5 as the improved APF method of local path planning of punctuation, when arrived at the second turning point, then P_6 as the next subtitle punctuation to continue the path planning until the USV reach the final point. Then, the loop ends. The algorithm flow is shown below and in Figure 11.

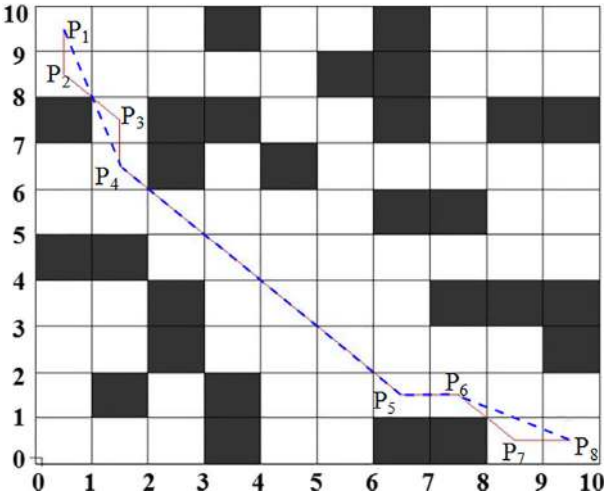

FIGURE 10. Improved ACO-APF hybrid algorithm global path planning.

Algorithm 1 The Improved Ant Colony Optimization - Artificial Potential Field Algorithm

1. Initialize input the parameters and environmental information such as target point, initial point into the USV.
2. Solve the initial path.
3. Simplify the initial path obtained by Step2
4. Applying the improved APF method for local path planning.
5. Determine whether the subhead punctuation is reached or not. If not reached, return to Step4; If so, enter Step6.
6. Determine whether the subhead punctuation is the final target point. If so, enter Step7; if not, select the next inflection point as subhead punctuation and return to Step4.
7. Complete path planning
8. End of the algorithm

$$k = \frac{x_o y_o + x_g y_g - x_g y_o - x_o y_g \pm r\sqrt{(-2y_o y_g - 2x_o x_g + y_g^2 + y_o^2 + x_o^2 - r^2 + x_g^2)}}{-r^2 + x^2 - 2x_o y_g + x_g^2} \tag{23}$$

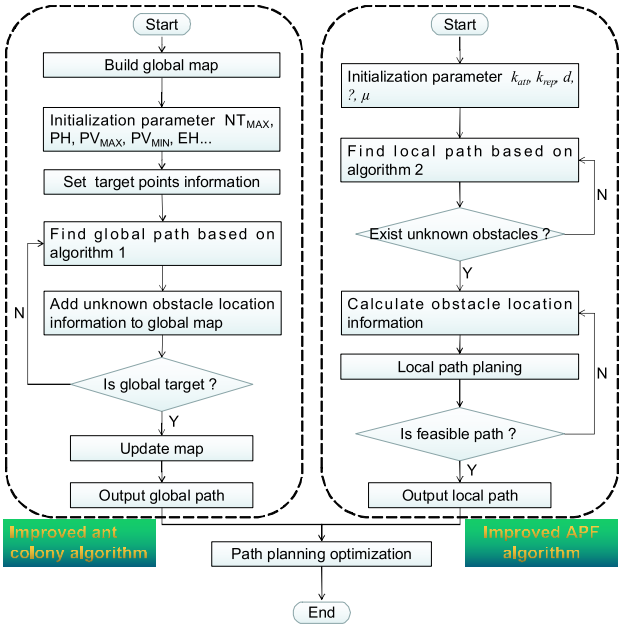

FIGURE 11. Improved ACO-APF algorithm flow chart.

TABLE 2. Parameter setting.

Parameter	Value	Parameter	Value
Maximum iteration number (NT_{MAX})	100	Number of ants	50
Maximum pheromone volatilization factor (PV_{MAX})	0.5	Minimum pheromone volatilization factor(PV_{MIN})	0.3
Pheromone heuristic (PH)	1	expected heuristic value (EH)	3

V. SIMULATION ANALYSIS

A. IMPROVED ACO ALGORITHM SIMULATION

1) 10 × 10 GRID MAP

A grid-scale is selected based on Equation 1. Based on the USV studied in this article, the selected L_{USV} is 1.5 m, $\bar{V}$ is 3.5 m/s, t_g is 3s, and ζ is 7. Simulation experiment 1 was carried out on a 10 × 10 grid map, with the initial point coordinate S (0.5, 9.5) and the target point coordinate G (9.5, 0.5). Because [36] describes a recent improved ACO algorithm that is indicative of those in the literature and is cited 116 times, so we conduct a simulation experiment by comparing this algorithm with the algorithm proposed in this study. The simulation parameters used in this experiment are shown in Table 2:

Figure 12 shows the optimal path planning curve solved by the three algorithms, and Figure 13 shows the convergence curve. The optimal paths of the three algorithms are shown to be identical; however, the proposed algorithm achieves the fastest convergence speed.

2) 20 × 20 GRID MAP

Simulation test 2 was performed on a 20 × 20 grid map with the initial and target point coordinates of (0.5,19.5) and (19.5,0.5), respectively. The parameter settings used in the simulation are shown in Table 3:

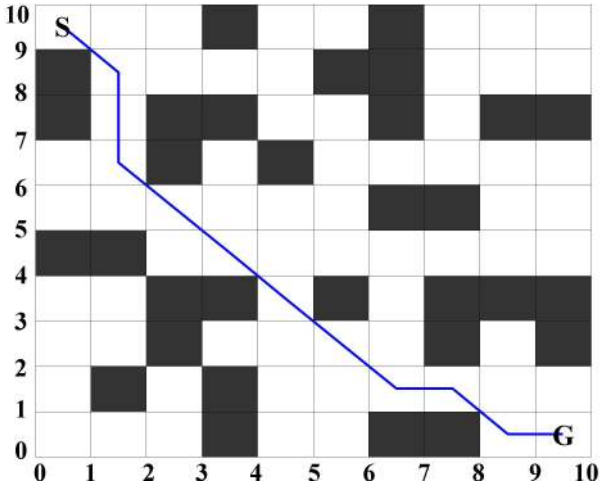

FIGURE 12. Optimal path of the USV solved by three algorithms.

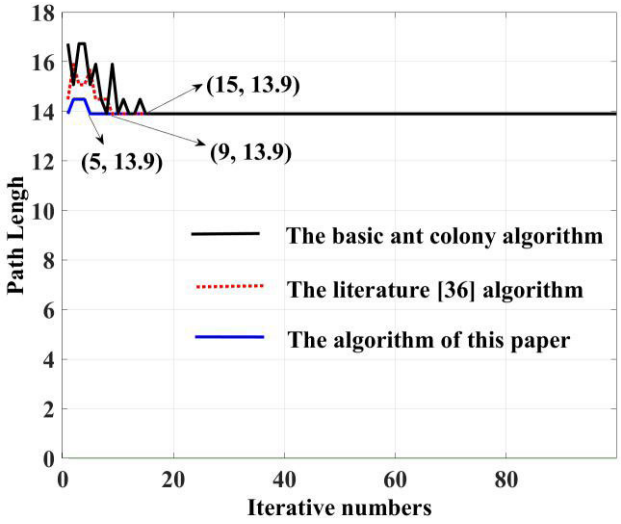

FIGURE 13. Convergence curves of the three algorithms.

TABLE 3. Parameter setting.

Parameter	Value	Parameter	Value
NT_{MAX}	100	Number of ants	50
PV_{MAX}	0.8	PV_{MIN}	0.3
PH	1	EH	6

Figure 14 shows the optimal path obtained by the three algorithms, and the meaning of these curves is consistent with Figure 13. The path calculated by the proposed algorithm is identical to that calculated by the algorithm in [36] and is better than that of the basic ACO algorithm.

Table 4 compares the results of the three algorithms. The proposed algorithm yields shorter path lengths, fewer iterations, and fewer inflection points, and can effectively search for a globally optimal path.

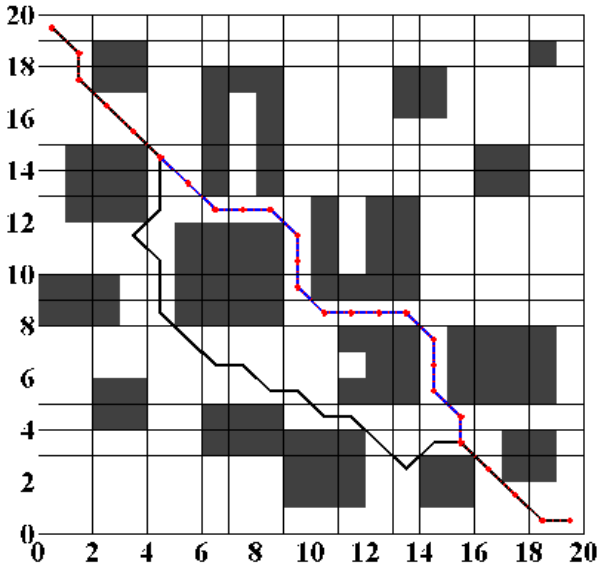

FIGURE 14. Optimal path of the USV solved by three algorithms.

TABLE 4. Simulation results of three algorithms.

Algorithm	Optimal path length/m	Number of iterations	Inflection point number
Traditional algorithm	32.97	18	17
Literature [36]	30.38	13	13
This paper	30.38	8	13

TABLE 5. Parameter setting.

Parameter	Value	Parameter	Value
NT_{MAX}	100	Number of ants	50
PV_{MAX}	0.8	PV_{MIN}	0.3
PH	1	EH	5.5

3) 30 × 30 GRID MAP

Simulation experiment 3 was conducted on a more complex 30 × 30 raster map, with the initial point coordinate S (0.5, 29.5). The settings of the parameters used in the simulation are shown in Table 5.

Figure 15 shows the optimal path, as determined by the three algorithms, and the meaning of the curve is consistent with Figure 13. From the figure that, the number of inflection points planned by the basic ACO algorithm, the algorithm in [36], and the proposed paper are 33, 20, and 11, respectively. The path curve planned by the proposed algorithm is thus better than the previous two.

Figure 16 shows the convergence curves of the three algorithms. In a complex environment, the convergence speed and path calculated by this algorithm are better than those of the other two algorithms. Table 6 shows that in a complex environment, the path length calculated by the algorithm in this article is 10% and 31% below those calculated by the algorithm in [36] and the basic ACO algorithm.

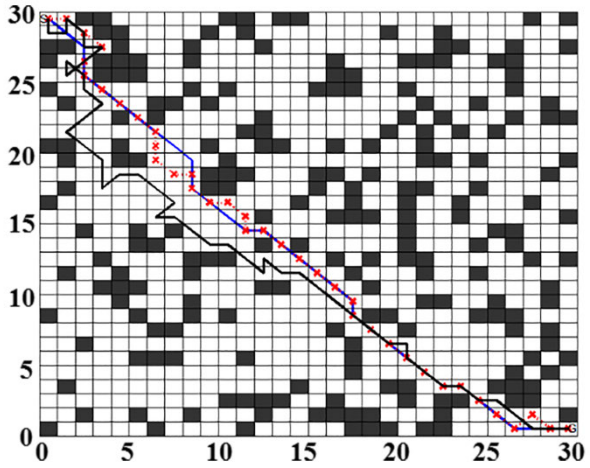

FIGURE 15. Optimal path of the USV solved by three algorithms.

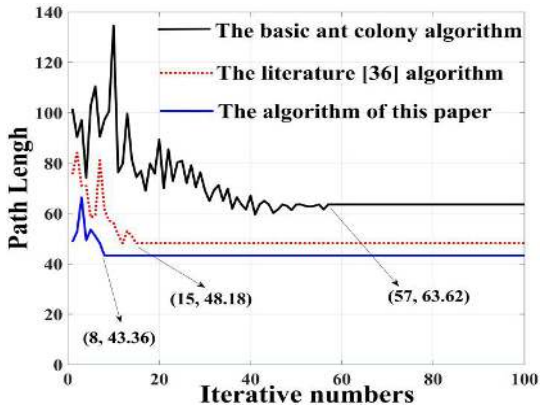

FIGURE 16. Convergence curves of the three algorithms.

TABLE 6. Simulation related parameter setting.

Algorithm	Optimal path length/m	Number of iterations	Inflection point number
Traditional algorithm	63.6	48.18	43.36
Literature [35]	57	15	8
This paper	33	20	11

The simulation results demonstrate that the global path planning capability of the improved ACO algorithm is better than the algorithm in [36] and the basic ACO algorithm. Because there are undiscovered areas in the working environment of USVs, and the ACO algorithm cannot perform local path planning, an improved APF method is proposed in this article to manage of uncharted obstacles.

B. IMPROVED APF ALGORITHM SIMULATION

1) SIMULATION RESULTS OF GNRON AND LOCAL MINIMUM POINT PROBLEM

To demonstrate the effect of the improved method of the APF method on the local minimum and the GNRON problem,

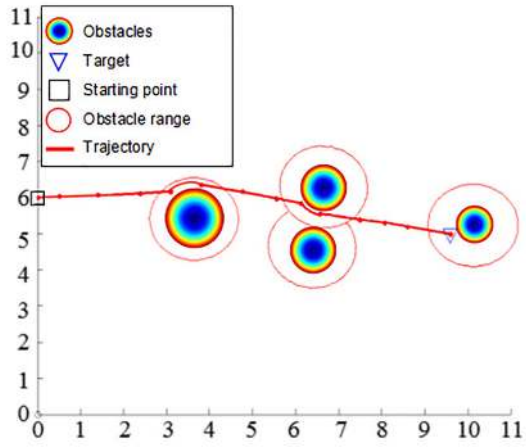

FIGURE 17. Simulation of GNRON and local minimum point.

TABLE 7. Contrast test.

	Ref.45	Ref.46	Ref.47	Ref.48	This paper
get to the target?	No	Yes	Yes	Yes	Yes
Is the path smooth?	Yes	Yes	Yes	No	Yes
Is force curve smooth?	Yes	No	No	No	Yes

the following simulation is performed. The initial point coordinates of the USV are (0,6); the coordinates of the three obstacles are (3.6,5.4), (6.3,4.5), and (6.5,6.5); and the target point coordinate is (9.7,5). The path planning results determined by the improved APF method are shown in Figure 17. The improved APF method can plan a path through the narrow channel between the two obstacles, enabling the USV to avoid the obstacles and reach the target successfully, thus solving the GNRON and the problem of the local minimum.

To verify the advanced nature of the algorithm proposed in this article, we compare the effect of this algorithm in solving GNRON with other algorithms. We compared the solution of the CNRON problem with the improved artificial potential field method proposed in [44]–[46]. Single obstacles were compared to those in [44]–[46], and multiple obstacles were compared to those in [47]. To increase the credibility of this comparison, the simulation environment was the same as the simulation environment mentioned in these references. Comparison results are shown in Table 7.

2) THE SIMULATION OF DYNAMIC STEP SIZE

A set of comparative simulation experiments are performed to demonstrate the effectiveness of dynamic step size adjustment. The simulation environment parameters are shown in Table 8, and the simulation results are shown in Figures 18 and 19.

Figures 18 and 19 show that the planned path of experiment 1 is 30 steps and that of experiment 2 is 16 steps. Dynamically

TABLE 8. System parameters.

	Test 1	Test 2
Step size	Fixed-step size：0.5	Dynamic step size：(0.5-1)
Coordinate	Initial point：(0,0) Obstacle：(1,1.5) (3,2.8) (6,2) (4,0.5) (5.5,5.5) (8,8.5) (5,8.5) (9,2.5) (9,5.5) Target point：(10,10)	

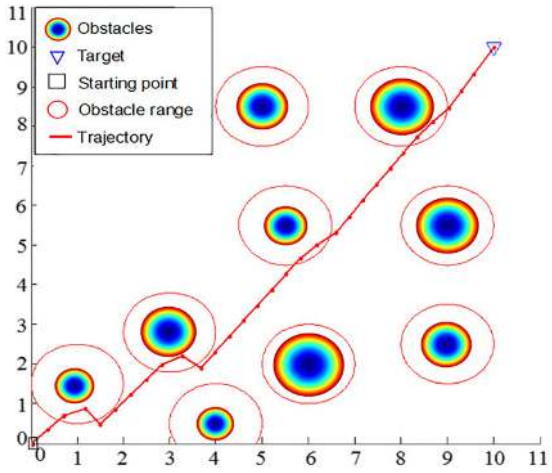

FIGURE 18. Path planned with a fixed step size.

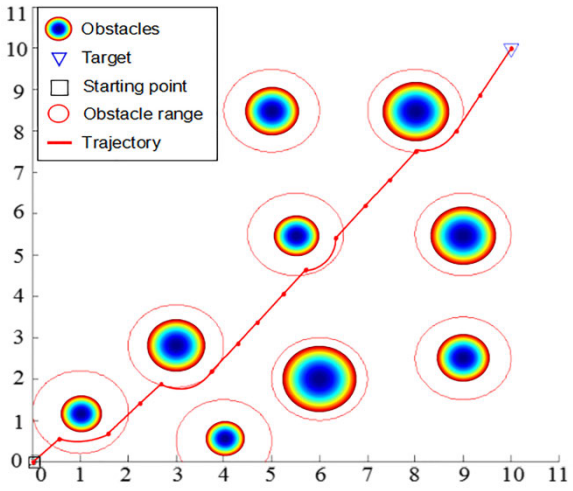

FIGURE 19. Path planned with a dynamic step size.

adjusting the step size can decrease computation time and produce a path that is smoother. Because the chosen path points are not interpolated or postprocessed using edge trimming or spline smoothing, they describe the true length of the path better. Thus, the path is not sufficiently smooth. In the future, we plan to choose a radius of the tangent circle that is based on a dynamics model of the USV's motion to make the path smoother.

C. SIMULATION OF IMPROVED ACO-APF HYBRID ALGORITHM

This article combines the improved ACO algorithm with the improved APF method to form the improved ant colony

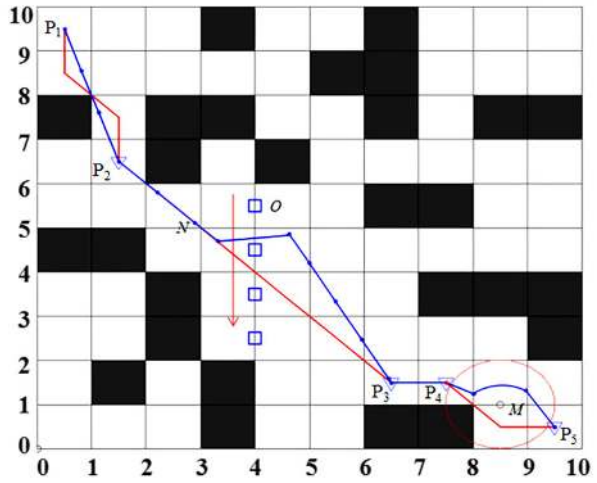

FIGURE 20. Simulation results of the proposed algorithm.

optimization-artificial potential field hybrid algorithm and performs a simulation test to establish the effectiveness of the algorithm in an uncharted environment. The simulation results are shown in Figure 20, in which the coordinates of the uncharted stationary obstacle are (8.5,1), the initial point of the moving obstacle *O* is (4,5.5), the initial point of the USV is (9.5,0.5), and the target point is (0.5,9.5). When the USV moves to point N, obstacle *O* begins to move vertically downward. In the figure, the solid lines in red and blue are global path planning and local path planning of the improved ACO-APF hybrid algorithm, respectively.

As shown in Figure 20, when using P3 as the subhead punctuation local path planning, after the USV moves to point N, obstacle *O* begins to move vertically downward. Then, the USV reduces the step size, avoids obstacle *O*, and moves to subhead punctuation P_3. When considering the local path planning of subhead punctuation P_5, the uncharted obstacle *M* appears in the USV's forward path, and the USV successfully avoids the uncharted obstacle *M* from arriving at the target through local path planning. Based on the simulation results, the improved ACO-APF hybrid algorithm local path planning can remain away from the undiscovered static and dynamic obstruction, and smooth the USV's path concurrently.

Programming the algorithm in C++ and implanting it into the USV controller for field testing to further demonstrate the proposed algorithm's reliability in a real environment.

VI. LAKE TEST

The proposed algorithm is used in the portable USV that is shown in Figure 21(a), which was developed by this study group. The hardware architecture of the USV is shown in Figure 21(b), and the primary parameters of the USV are shown in Table 9. The wireless bridge provides communication between the USV and workstations. With the thruster powered by 24 V DC, the speed of the USV is 2.08 kn. LiDAR is installed on the USV to detect uncharted

TABLE 9. Primary parameters of the USV.

Size	0.53 × 1.56 m
Navigation Speed	2~6Kn
continuation of the journey	6 h@4Kn
Heading Angle	-30°
Rudder angle	≦30°
Turning Radius	0.5 m

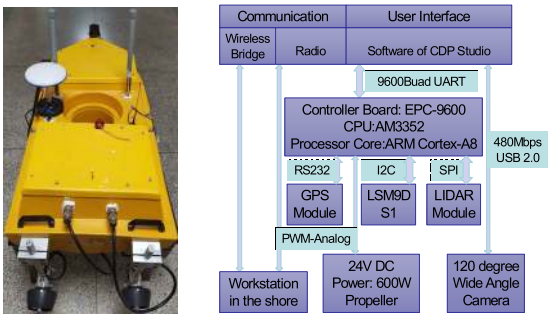

(a)USV for the test. (b) The hardware architecture of the USV.

FIGURE 21. Test platform.

obstacles, and median filtering is used to process the data.

In practical experiments, the influence of water flow cannot be ignored. For the water flow, the velocity synthesis method proposed in [48] is used to enable the USV to overcome the influence of water flow disturbance. The USV's anti-interference calculations are managed by its dynamic control unit, which is not the focus of this article.

Before the test, a map of the test water area was pre-treated using the raster method. In the field tests, the USV first follows the prior global path of the algorithm method. When the LiDAR finds an uncharted obstacle, the coordinates of the obstacle are calculated based on the relative position of the USV and the obstacle, and obstacle avoidance is planned using the local path. After obstacle avoidance, the USV still sails based on the global path. During the field tests, the USV track is drawn, and the GPS points obtained are shown in Figures 22 and 23; Figure 24 shows the distance error between the two paths; and the field test is shown in Figure 25. By comparing the ideal data with the real data of the experimental data, errors are shown to reach 10 m, and large errors occur during turning and local obstacle avoidance. However, considering the maneuverability of the USV and the effects of environmental factors, particularly the wind, the results are acceptable. The ideal length for planning the USV road force is 350 meters, and the total experimental path length is 322.5 meters, indicating an error of 27.5 meters or 4%. The positioning error of the USV during navigation is primarily caused by GPS, which has an error of 3 meters. Videos of the experiment can be found at https://v.youku.com/v_show/id_XNDgyODI0NDg0OA==.html?firsttime=68. The simulation and field test indicate that this algorithm can effectively plan the USV's global path and avoid obstacle.

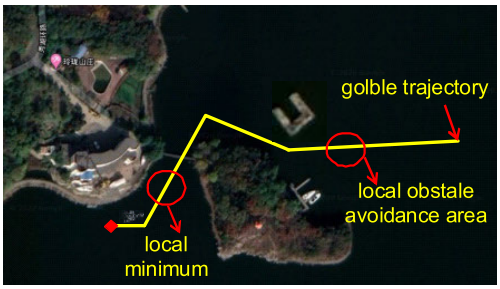

FIGURE 22. Map of real-world testing at the Qipanshan reservoir.

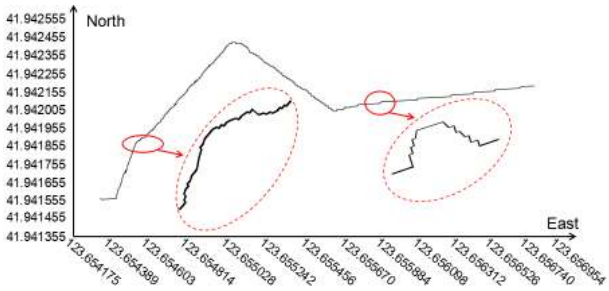

FIGURE 23. GPS points during the experiment.

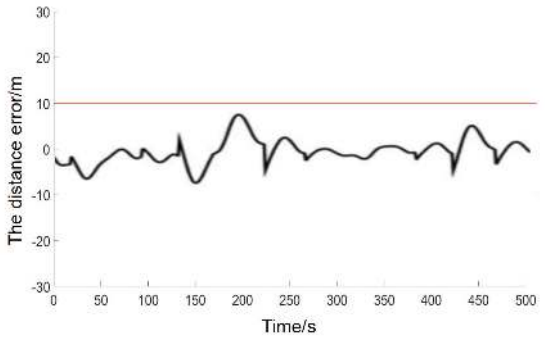

FIGURE 24. Distance error.

(a) USV rides the waves. (b) The USV avoids uncharted obstacles

FIGURE 25. Results of the field test.

VII. CONCLUSION

USV path planning and obstacle avoidance based on an improved ACO-APF hybrid algorithm with adaptive early warning is presented for use in a complex environment. USV path planning is divided into three aspects: environmental modeling; path search and optimization; and obstacle avoidance. This article uses the grid method to model the environment. The improved ACO algorithm is used for global path planning and proposes a new heuristic function, the pheromone update rule, and the dynamic pheromone volatilization factor. Simulation results show that in the 30*30 grid, the optimal path length is 51.6% of the traditional ACO algorithm, and the number of iterations is 43.3%. To solve the problem that global path planning cannot avoid undiscovered obstacles, we use the improved APF algorithm to perform local path planning and solve the problem of undiscovered targets and local minima in the classical algorithm, and the step length is optimized with a dynamic warning mechanism. This article combined two improved algorithms to form the improved ACO-APF hybrid algorithm. Simulation results demonstrate that the proposed method can efficiently find the optimal path and effectively avoid uncharted static and dynamic obstacles. Finally, a USV surface path planning experiment is performed, and the results indicate that the proposed algorithm can calculate path planning efficiently and accurately in a complex surface environment.

REFERENCES

[1] J. Sun, J. Tang, and S. Lao, "Collision avoidance for cooperative UAVs with optimized artificial potential field algorithm," *IEEE Access*, vol. 5, pp. 18382–18390, Aug. 2017, doi: 10.1109/ACCESS.2017.2746752.

[2] J. Tang, "Conflict detection and resolution for civil aviation: A literature survey," *IEEE Aerosp. Electron. Syst. Mag.*, vol. 34, no. 10, pp. 20–35, Oct. 2019, doi: 10.1109/MAES.2019.2914986.

[3] M. Breivik, V. E. Hovstein, and T. I. Fossen, "Straight-line target tracking for unmanned surface vehicles," *Model., Identificat. Control, Norwegian Res. Bull.*, vol. 29, no. 4, pp. 131–149, 2008, doi: 10.4173/mic.2008.4.2.

[4] W. Naeem, T. Xu, R. Sutton, and A. Tiano, "The design of a navigation, guidance, and control system for an unmanned surface vehicle for environmental monitoring," *Proc. Inst. Mech. Eng., M, J. Eng. Maritime Environ.*, vol. 222, no. 2, pp. 67–79, Jun. 2008, doi: 10.1243/14750902jeme80.

[5] R. Sutton, S. Sharma, and T. Xao, "Adaptive navigation systems for an unmanned surface vehicle," *J. Mar. Eng. Technol.*, vol. 10, no. 3, pp. 3–20, Sep. 2011, doi: 10.1080/20464177.2011.11020248.

[6] B. Bingham, N. Kraus, B. Howe, L. Freitag, K. Ball, P. Koski, and E. Gallimore, "Passive and active acoustics using an autonomous wave glider," *J. Field Robot.*, vol. 29, no. 6, pp. 911–923, Nov. 2012, doi: 10.1002/rob.21424.

[7] S. Campbell, W. Naeem, and G. W. Irwin, "A review on improving the autonomy of unmanned surface vehicles through intelligent collision avoidance manoeuvres," *Annu. Rev. Control*, vol. 36, no. 2, pp. 267–283, Dec. 2012, doi: 10.1016/j.arcontrol.2012.09.008.

[8] H. Niu, Y. Lu, A. Savvaris, and A. Tsourdos, "An energy-efficient path planning algorithm for unmanned surface vehicles," *Ocean Eng.*, vol. 161, pp. 308–321, Aug. 2018, doi: 10.1016/j.oceaneng.2018.01.025.

[9] P. Marin-Plaza, A. Hussein, D. Martin, and A. D. L. Escalera, "Global and local path planning study in a ROS-based research platform for autonomous vehicles," *J. Adv. Transp.*, vol. 2018, pp. 1–10, Feb. 2018, doi: 10.1155/2018/6392697.

[10] W. R. Uttal, "Artificial intelligence and mobile robots," *J. Math. Psychol.*, vol. 43, no. 1, pp. 155–164, Mar. 1999, doi: 10.1006/jmps.1998.1238.

[11] C. Cai and S. Ferrari, "Information-driven sensor path planning by approximate cell decomposition," *IEEE Trans. Syst., Man, Cybern. B. Cybern.*, vol. 39, no. 3, pp. 672–689, Jun. 2009, doi: 10.1109/tsmcb.2008.2008561.

[12] L. Xie, S. Xue, J. Zhang, M. Zhang, W. Tian, and S. Haugen, "A path planning approach based on multi-direction A* algorithm for ships navigating within wind farm waters," *Ocean Eng.*, vol. 184, pp. 311–322, Jul. 2019, doi: 10.1016/j.oceaneng.2019.04.055.

[13] Z. Shen, J. P. Wilson, and S. Gupta, "An online coverage path planning algorithm for curvature-constrained AUVs," in *Proc. OCEANS MTS/IEEE SEATTLE*, Seattle, WA, USA, Oct. 2019, pp. 1–5.

[14] A. L. Song, B. Y. Su, C. Z. Dong, D. W. Shen, E. Z. Xiang, and F. P. Mao, "A two-level dynamic obstacle avoidance algorithm for unmanned surface vehicles," *Ocean Eng.*, vol. 170, pp. 351–360, Dec. 2018, doi: 10.1016/j.oceaneng.2018.10.008.

[15] J. Li, G. Deng, C. Luo, Q. Lin, Q. Yan, and Z. Ming, "A hybrid path planning method in unmanned Air/Ground vehicle (UAV/UGV) cooperative systems," *IEEE Trans. Veh. Technol.*, vol. 65, no. 12, pp. 9585–9596, Dec. 2016, doi: 10.1109/tvt.2016.2623666.

[16] Q. Pan and X. Wang, "Independent travel recommendation algorithm based on analytical hierarchy process and simulated annealing for professional tourist," *Appl. Intell.*, vol. 48, no. 6, pp. 1565–1581, Jun. 2018, doi: 10.1007/s10489-017-1014-0.

[17] Y.-N. Ma, Y.-J. Gong, Y. Gao, J. Zhang, and C.-F. Xiao, "Path planning for autonomous underwater vehicles: An ant colony algorithm incorporating alarm pheromone," *IEEE Trans. Veh. Technol.*, vol. 68, no. 1, pp. 141–154, Jan. 2019, doi: 10.1109/tvt.2018.2882130.

[18] J. Sheng, G. He, J. Li, and W. Guo, "An improved artificial potential field algorithm for virtual human path planning," in *Proc. Int. Conf. Entertainment Educ. Digit. Techn. Syst.*, Changchun, China, vol. 6249, Aug. 2010, pp. 2–337.

[19] R. Mur-Artal, J. M. M. Montiel, and J. D. Tardos, "ORB-SLAM: A versatile and accurate monocular SLAM system," *IEEE Trans. Robot.*, vol. 31, no. 5, pp. 1147–1163, Oct. 2015, doi: 10.1109/tro.2015.2463671.

[20] J. Baltes, D. W. Kung, and W. Y. Wang, "Adaptive computational SLAM incorporating strategies of exploration and path planning," *Knowl. Eng. Rev.*, vol. 34, no. e23, Dec. 2019, doi: 10.1017/s0269888919000183.

[21] I. Maurovic, M. Seder, K. Lenac, and I. Petrovic, "Path planning for active SLAM based on the D* algorithm with negative edge weights," *IEEE Trans. Syst., Man, Cybern. Syst.*, vol. 48, no. 8, pp. 1321–1331, Aug. 2018, doi: 10.1109/tsmc.2017.2668603.

[22] J. Clemens, T. Reineking, and T. Kluth, "An evidential approach to SLAM, path planning, and active exploration," *Int. J. Approx. Reasoning*, vol. 73, pp. 1–26, Jun. 2016, doi: 10.1016/j.ijar.2016.02.003.

[23] A. Palomer, P. Ridao, and D. Ribas, "Inspection of an underwater structure using point-cloud SLAM with an AUV and a laser scanner," *J. Field Robot.*, vol. 36, no. 8, pp. 1333–1344, Dec. 2019, doi: 10.1002/rob.21907.

[24] J. R. Garcia, J. A. Farrell, Z. M. Kassas, and M. T. Ouimet, "Autonomous surface vehicle multistep look-ahead measurement location planning for optimal localization of underwater acoustic transponders," *IEEE Trans. Aerosp. Electron. Syst.*, vol. 55, no. 6, pp. 2836–2849, Dec. 2019, doi: 10.1109/taes.2019.2909253.

[25] X. Liu, Y. Li, J. Zhang, J. Zheng, and C. Yang, "Self-adaptive dynamic obstacle avoidance and path planning for USV under complex maritime environment," *IEEE Access*, vol. 7, pp. 114945–114954, 2019, doi: 10.1109/access.2019.2935964.

[26] A. Sgorbissa and R. Zaccaria, "Planning and obstacle avoidance in mobile robotics," *Robot. Auto. Syst.*, vol. 60, no. 4, pp. 628–638, Apr. 2012, doi: 10.1016/j.robot.2011.12.009.

[27] A. Lazarowska, "Comparison of discrete artificial potential field algorithm and wave-front algorithm for autonomous ship trajectory planning," *IEEE Access*, vol. 8, pp. 221013–221026, 2020, doi: 10.1109/access.2020.3043539.

[28] O. Montiel, U. Orozco-Rosas, and R. Sepulveda, "Path planning for mobile robots using bacterial potential field for avoiding static and dynamic obstacles," *Expert Syst. Appl.*, vol. 42, no. 12, pp. 5177–5191, Jul. 2015, doi: 10.1016/j.eswa.2015.02.033.

[29] D. Zhao, H. Yu, X. Fang, L. Tian, and P. Han, "A path planning method based on multi-objective cauchy mutation cat swarm optimization algorithm for navigation system of intelligent patrol car," *IEEE Access*, vol. 8, pp. 151788–151803, 2020, doi: 10.1109/access.2020.3016565.

[30] B. Shuang, J. Chen, and Z. Li, "Study on hybrid PS-ACO algorithm," *Appl. Intell.*, vol. 34, no. 1, pp. 64–73, Feb. 2011, doi: 10.1007/s10489-009-0179-6.

[31] M.-C. Tsou, "Multi-target collision avoidance route planning under an ECDIS framework," *Ocean Eng.*, vol. 121, pp. 268–278, Jul. 2016, doi: 10.1016/j.oceaneng.2016.05.040.

[32] Q. Zhang and B. K. Chen, "Ant colony optimization with improved potential field heuristic for robot path planning," *Trans. Chin. Soc. Agricult. Machinery*, vol. 50, no. 5, pp. 23–32, May 2019, doi: 10.6041/j.issn.1000-1298.2019.05.003.

[33] D. B. Zhao and J. Q. Yi, "Robot planning with artificial potential field guided ant colony optimization algorithm," in *Proc. 2nd Int. Conf. Natural Comput.*, Xi'an, China, vol. 4222, Sep. 2006, pp. 222–231.

[34] G. Che, L. Liu, and Z. Yu, "An improved ant colony optimization algorithm based on particle swarm optimization algorithm for path planning of autonomous underwater vehicle," *J. Ambient Intell. Humanized Comput.*, vol. 11, no. 8, pp. 3349–3354, Aug. 2020, doi: 10.1007/s12652-019-01531-8.

[35] G. Han, Z. Zhou, T. Zhang, H. Wang, L. Liu, Y. Peng, and M. Guizani, "Ant-colony-based complete-coverage path-planning algorithm for underwater gliders in ocean areas with thermoclines," *IEEE Trans. Veh. Technol.*, vol. 69, no. 8, pp. 8959–8971, Aug. 2020, doi: 10.1109/tvt.2020.2998137.

[36] X. L. Hou and L. Z. Yu, "Mobile robot path planning based on improved ant colony algorithm," (In Chinese), *Softw. Guide*, vol. 16, no. 12, pp. 166–168, 2017.

[37] E. G. Tsardoulias, A. Iliakopoulou, A. Kargakos, and L. Petrou, "A review of global path planning methods for occupancy grid maps regardless of obstacle density," *J. Intell. Robot. Syst.*, vol. 84, nos. 1–4, pp. 829–858, Dec. 2016, doi: 10.1007/s10846-016-0362-z.

[38] Y. Fujii, "A definition of the evasive domain," *Jpn. Inst. Navigat.*, vol. 65, pp. 17–22, Sep. 1980.

[39] S. Piotr, "Course control of unmanned surface vehicle," *Solid State Phenomena*, vol. 196, pp. 117–123, Feb. 2013.

[40] Z. Fan and H. Li, "Two-layer model predictive formation control of unmanned surface vehicle," in *Proc. Chin. Autom. Congr. (CAC)*, Jinan, China, Oct. 2017, pp. 6002–6007.

[41] F. Yunsheng, S. Xiaojie, W. Guofeng, and G. Chen, "On fuzzy self-adaptive PID control for USV course," in *Proc. 34th Chin. Control Conf.*, Chicago, IL, USA, Jul. 2015, pp. 8472–8478.

[42] M. Caccia, M. Bibuli, R. Bono, and G. Bruzzone, "Basic navigation, guidance and control of an unmanned surface vehicle," *Auto. Robots*, vol. 25, no. 4, pp. 349–365, Nov. 2008, doi: 10.1007/s10514-008-9100-0.

[43] S. Xie, P. Wu, H. Liu, P. Yan, X. Li, J. Luo, and Q. Li, "A novel method of unmanned surface vehicle autonomous cruise," *Ind. Robot, Int. J.*, vol. 43, no. 1, pp. 121–130, Jan. 2016, doi: 10.1108/ir-05-2015-0097.

[44] Y. Koren and J. Borenstein, "Potential field methods and their inherent limitations for mobile robot navigation," in *Proc. IEEE Int. Conf. Robot. Autom.*, Dec. 1991, pp. 1398–1404.

[45] S. S. Ge and Y. J. Cui, "New potential functions for mobile robot path planning," *IEEE Trans. Robot. Autom.*, vol. 16, no. 5, pp. 615–620, Oct. 2000.

[46] H. H. Triharminto, "A novel of repulsive function on artificial potential field for robot path planning," *Int. J. Electr. Comput. Eng.*, vol. 6, no. 6, pp. 3262–3275, Dec. 2016, doi: 10.11591/ijece.v6i6.pp3262-3275.

[47] L.-X. Yang, Z. X. Liu, and H. Tang, "A novel approach for path planning based on reactive behavior-artificial potential filed," *Appl. Mech. Mater.*, vol. 529, pp. 646–649, Jun. 2014, doi: 10.4028/www.scientific.net/AMM.529.646.

[48] X. Cao, D. Zhu, and S. X. Yang, "Multi-AUV target searching under ocean current based on PPSO and velocity synthesis algorithm," *Underwater Technol.*, vol. 33, no. 1, pp. 31–39, Jul. 2015, doi: 10.3723/ut.33.031.

YANLI CHEN received the B.E. degree in mechatronic engineering from Jiamusi University, Jiamusi, China, in 2007, and the M.E. and Ph.D. degrees in mechatronics engineering from Jilin University, Changchun, China, in 2009 and 2012, respectively. He was a Postdoctoral Research Worker in solid geophysics with Jilin University, in 2016. He is currently an Associate Professor. His research interests cooperatively pursue and intelligent control of multiple autonomous underwater vehicles, fluid power transmission, and control.

GUIQIANG BAI received the B.E. degree in mechanical design manufacture and automation from Yantai University, China, in 2016, and the M.E. degree in mechatronic engineering from the Shenyang Institute of Automation, Chinese Academy of Sciences, Shenyang, China, in 2019. He is currently pursuing the Ph.D. degree with Jilin University, Changchun, China. His research interests include recovery and intelligent control of UUV, and cooperatively pursue and intelligent control of multiple autonomous underwater vehicles.

YIN ZHAN received the M.E. degree in mechatronics engineering from Jilin University, Changchun, China, in 2020. His research interests include recovery and intelligent control of UUV, and cooperatively pursue and intelligent control of multiple autonomous underwater vehicles.

XINYU HU received the B.E. degree in mechanical design manufacture and automation from Northeast University, Qinhuangdao, China, in 2017, and the M.E. degree in mechatronic engineering from the CSIC 710 Institute, in 2020. He is currently pursuing the Ph.D. degree with Jilin University, Changchun, China. His research interests include recovery and intelligent control of UUV, and cooperatively pursue and intelligent control of multiple autonomous underwater vehicles.

JUN LIU (Student Member, IEEE) received the B.E. degree in computer science from Wuhan University, Wuhan, China, in 2002, and the Ph.D. degree in computer science and engineering from the University of Connecticut, Connecticut, USA, in 2013. He is currently a Professor at Beihang University. His main research interests include embedded sensor networks, artificial intelligence and big data applications, and virtual reality technology.